ANALYSIS AND CRITIQUE OF THE ENVELOPE-TRACING METHOD FOR THE INVESTIGATION OF SOLAR PROMINENCES

by

John Anthony Cape

A THESIS

Submitted to the Graduate Faculty

in

partial fulfillment of the requirements

for the degree of

Master of Science in Engineering Physics

at

Montana State College

Approved:

Head, Major Department

Chairman, Examining Committee

Dean, Graduate Division

Bozeman, Montana
June, 1953

TABLE OF CONTENTS

ABSTRACT

A method of studying solar prominence motion, wherein the outlines of an eruptive prominence are traced from photographic film at successive intervals of time by means of a specially designed projector, is described. The motion of the prominence in the x and y directions is then plotted against the time and the resulting curves analyzed by means of a curve fitting procedure due to Birge. Results indicate that, excepting large probable error, the acceleration of the prominence, in the eruption stage, is very nearly constant both in the x and y directions for the relatively short time interval during which measurements are taken. Main source of error is found to be the measurement of heights above the chromosphere, due to non-uniform centering of the occulting disk of the coronagraph with successive exposures.

INTRODUCTION

When, in 1931, the French astronomer, Bernard Lyot, first photographed the solar corona without the aid of a total eclipse, but by means of his newly developed coronagraph, it was apparent that astronomers had at last been given the instrument which would permit extensive research in the study of solar prominences and other interesting features which appeared within the corona itself. Only in recent years have some of these instruments been constructed in observatories at Climax, Colorado; Pic du Midi in the Pyrenees; Sacramento Peak, New Mexico; Arosa, Switzerland; Wendelstein, Bavaria; Kanzelhöhe, Austria; Mt. Norikura, Japan and a Russian station somewhere in the Caucasus.

Observational data concerning the solar corona, which has been supplied by these observatories, consist primarily of motion pictures of prominence activity. Perhaps more than 50,000 feet of film have been exposed at these various stations, with more than 20,000 feet from Climax alone.

To date, analysis of these films has consisted primarily of tracing the motion of well defined "knots" and "streamers". The method has been quite successful but has, nevertheless, had many shortcomings. One particular difficulty is that usually rather few "well defined" knots or streamers can be found which remain sharp and clear for an appreciable period of time. The disappearance and reappearance of prominence features is a familiar phenomenon,[1] although it usually occurs most noticeably in

1. Dodson and McMath, 1948 (11), have given evidence of a filament which disappeared and then reappeared. Others have claimed to have witnessed the same phenomenon.

the case of delicate streamers and knots which are quite tenuous to begin with.

The acquisition, by the Climax Observatory, of a projector which permits highly magnified and distortion-free pictures to be focused on graph paper with fine resolution, has suggested a new mode of study of the prominence motion. This new method is concerned with tracing the general outline or envelope of the prominence or certain prominence features, at successive intervals of time (usually equally spaced), and then proceeding to extract information from these curves. The idea is based on the supposition that the succeeding envelopes of the prominence motion should tend to become aligned with the equipotential surfaces of the force field; and that motion outward orthogonal to the envelope should indeed be along the lines of force. It is apparent then that, should this situation be realized, it is only a matter of measurement to obtain information on the force field.

This investigation proposes to examine one solar prominence by this method, and to give not only as much information about the forces and velocities as is measurable, but also to serve as a general critique of the method, specifying quantitatively, whenever possible, the general accuracy of the method and attempting to point out its shortcomings.

As might be expected, the envelopes traced (see figure 6) are rough and full of humps as the prominence itself appears; and hence it would seem that they are certainly not equipotential surfaces. Obviously, then, there is a large element of human judgment in assigning the

directions of the lines of force. In this particular investigation, the measurements are confined to two areas, one in which the motion was entirely vertical and the other in which the motion was transverse.

DESCRIPTION OF THE PROMINENCE

The solar prominence with which this investigation is concerned appeared over the southeastern limb of the sun on September 8, 1948. It was of the eruptive type, and was photographed with the coronagraph of the High Altitude Observatory of Harvard University and the University of Colorado at Climax, Colorado from 16:29 to 20:23 U.T. on September 8, 1948, at the rate of one picture per half minute. The measurements and data presented herein are concerned chiefly with the period $17^h45.5^m$ to 18^h15^m, a relatively brief episode in the life of the prominence, during which virtually the entire eruptive motion took place. The northern-most and southern-most extremities of the arch lay at approximately -23° and -44.5° heliographic latitude, respectively, and at approximately 330° heliograph longitude. A large bipolar sunspot (Mt. Wilson No. 9395) lay 1° south and roughly 10° west of the northern extremity. This was a relatively short-lived spot, since it was first seen September 8 and was classified 1βd at that time.[2]

A large bipolar group (Mt. Wilson No. 9400), classified 1βpl, was

---

2. Sunspots are classified as follows:
   β = bipolar members; approximately equal in size.
   βp = bipolar members; preceding member dominant.
   βf = bipolar members; following member dominant.
   γ = composite spots.
   γβ = composite spots with leading members bipolar.
   l = living.
   d = dead or dying; i.e., 1βd = living when first seen; dead or dying when last seen . . .
   See: Menzel, Donald H., OUR SUN, Blakiston's Sons and Company, Philadelphia, 1949.

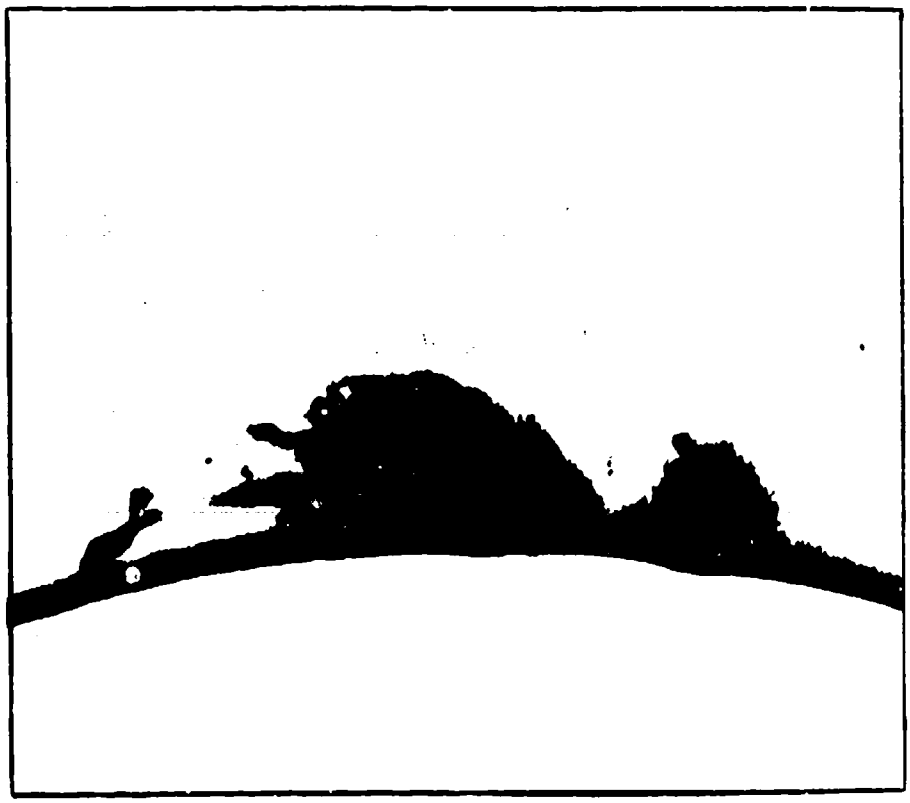

Figure 1. The prominence as it appeared when first observed (16^h30^m U.T.). Rapid upward motion or eruption has already commenced. The sunspots are at the extreme northern (left) end of the arch. At this time, matter seemed to be moving in that direction.

situated very near the northern tip of the arch, being roughly 3° south of it. The prominence, as it appeared when first seen, is picturedin figure 1. At this time (16^h30^m), it was already in the process of slow expansion with acceleration. By 17^h40^m, it had formed into a characteristic arch (figure 2) in which material was streaming into the phcto-sphere along both ends. The prominence continued to rise and expand with increasing velocity, meanwhile developing into a well-defined loop as is illustrated in figures 3 and 4, and reaching a height of 400,000 kilometers (figure 4), at which time its upward velocity was in excess of 250 kms/sec. Thereafter, its upper portions became diffuse and disappeared from view. Matter continued to descend along the arches, particularly the southern-most, the northern arch having virtually disappeared by this time; so that by 19^h00^m there remained only two bright mounds of material at the extremities (figure 5).

The apparent[3] motion of material along the arches very strongly suggests that the extremities were indeed strong centers of attraction. This was true particularly of the southern-most, though there were no sunspots known to be near that end. On the contrary, a very large spot concentration was found near the northern extreme of the arch where matter visibly streaming downward was barely perceptible and fading. Now,

---

3. The word "apparent" is employed here to describe the motion because there has been no little conjecture as to whether material is actually moving or whether the effect is merely the result of moving excitation fields or some such phenomena. For example, consider the motion of a beam of light along a mass of clouds. Dodson and Weston (1950) have found significant evidence in favor of the hypothesis of moving material.

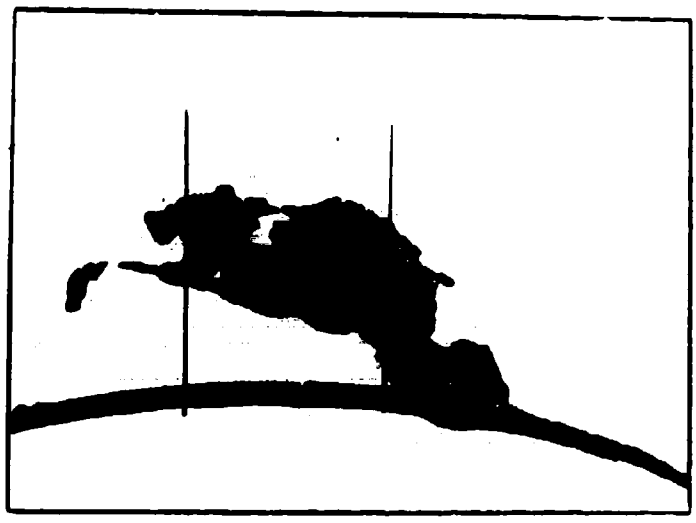

Figure 2. The prominence at 17^h40^m U.T. The region between the parallel lines is the region in which the motion of the envelope is measured and plotted (see figures 7 to 14). At this time matter appears to be streaming downward along the arches.

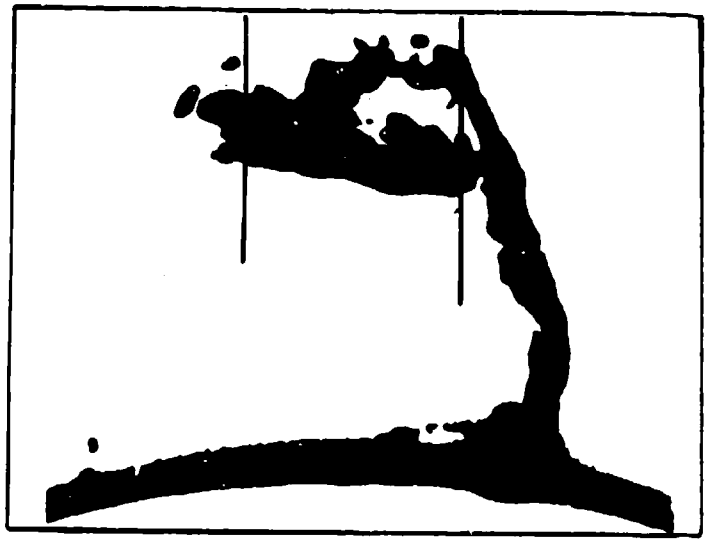

Figure 3. The prominence at 18^h00^m U.T. Note the gradual formation of the looplike arch.

streaming into the sun along this arch, there might very well have been large quantities of matter which was simply invisible. The prominences are known to be composed almost entirely of hydrogen and to be visible due to the fact that the gas is radiating. Some observers (among them, Dodson and McMath, 1948 - see footnote no. 1) have given evidence for prominence features which are at times visible and at other times not. The assumption that some matter in the prominence is invisible at times is a generally accepted one.

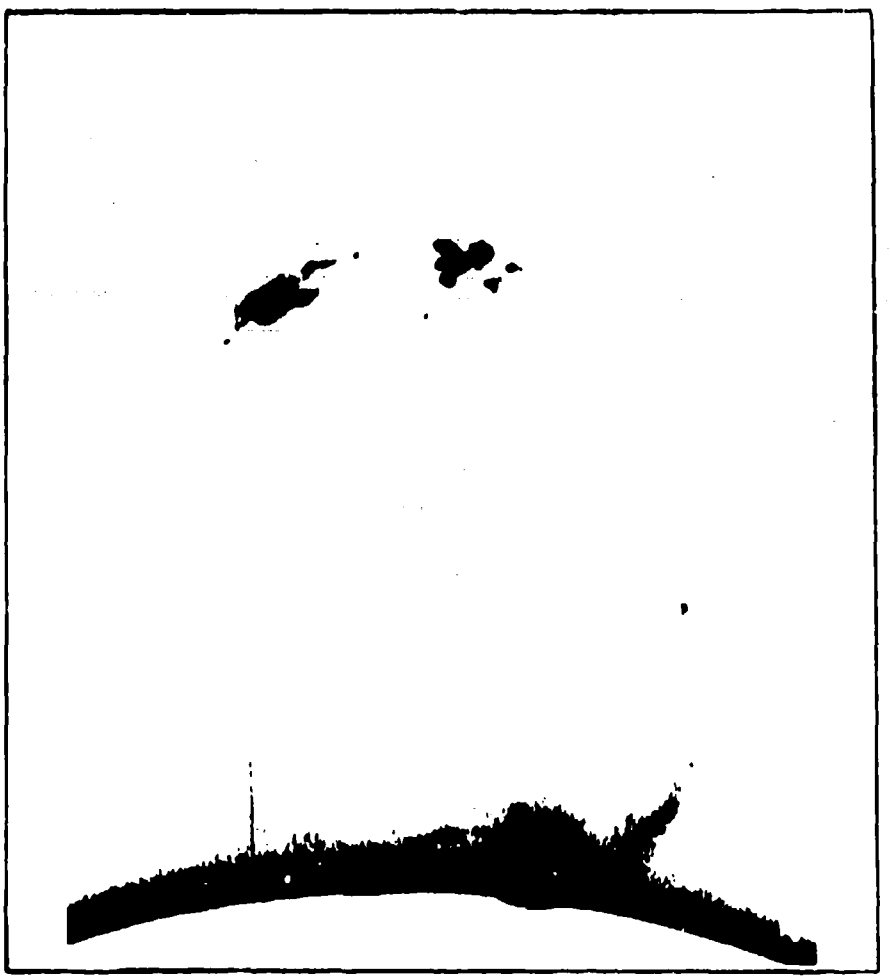

Figure 4. The prominence at 18^h15^m U.T. Unfortunately, reproduction of the photographs has caused the loss of much detail. On the original film, the southern (right) branch of the arch is very nearly intact although quite tenuous. Material has been rapidly dispersing. The vertical velocity at this time is approximately 250 kms/sec.

Figure 5. The prominence at 19^h00^m U. T. The material visible at the top of figure 4 has risen out of the scope of the camera. The two mounds of material shown here remained this way for more than an hour.

PLOTTING THE PROMINENCE MOTION

With the aid of the specially designed projector, selected frames from the film, chosen at equal intervals of time, have been traced on graph paper (figure 6). The pictures are "blown up" to a scale of 1 mm. to 1.39×10^3 kms., which corresponds to a solar radius of 50 cms. on the graph paper. In the rectangular system of coordinates, here employed, the origin is located on the solar limb at -37° heliographic latitude with the x-axis tangent to the limb at that point. We thus have a graph, scaled in distance and time, from which we can obtain measurements to study the motion of the prominence and the forces producing this motion. We shall not enter into any speculation as to the type of force field or fields involved, but shall attempt quantitative measurements.

Consider, for example, figure 7 and imagine a smooth curve drawn through the points so that for any instant of time t, the corresponding ordinate on the curve gives the y position (height) of the point on the envelope of the prominence whose x position is zero (in this particular case). In other words, the equation of the curve, call it y (t), describes the motion of a point on the envelope of the prominence which has always the abscissa x = 0. The "best fit" curve through these points was obtained by the orthogonal polynomial least squares method of curve fitting as adapted by Birge[4] and Weinberg (4). The result was the

4. For the sake of brevity, throughout the remainder of this paper the method shall be referred to as the Birge method.

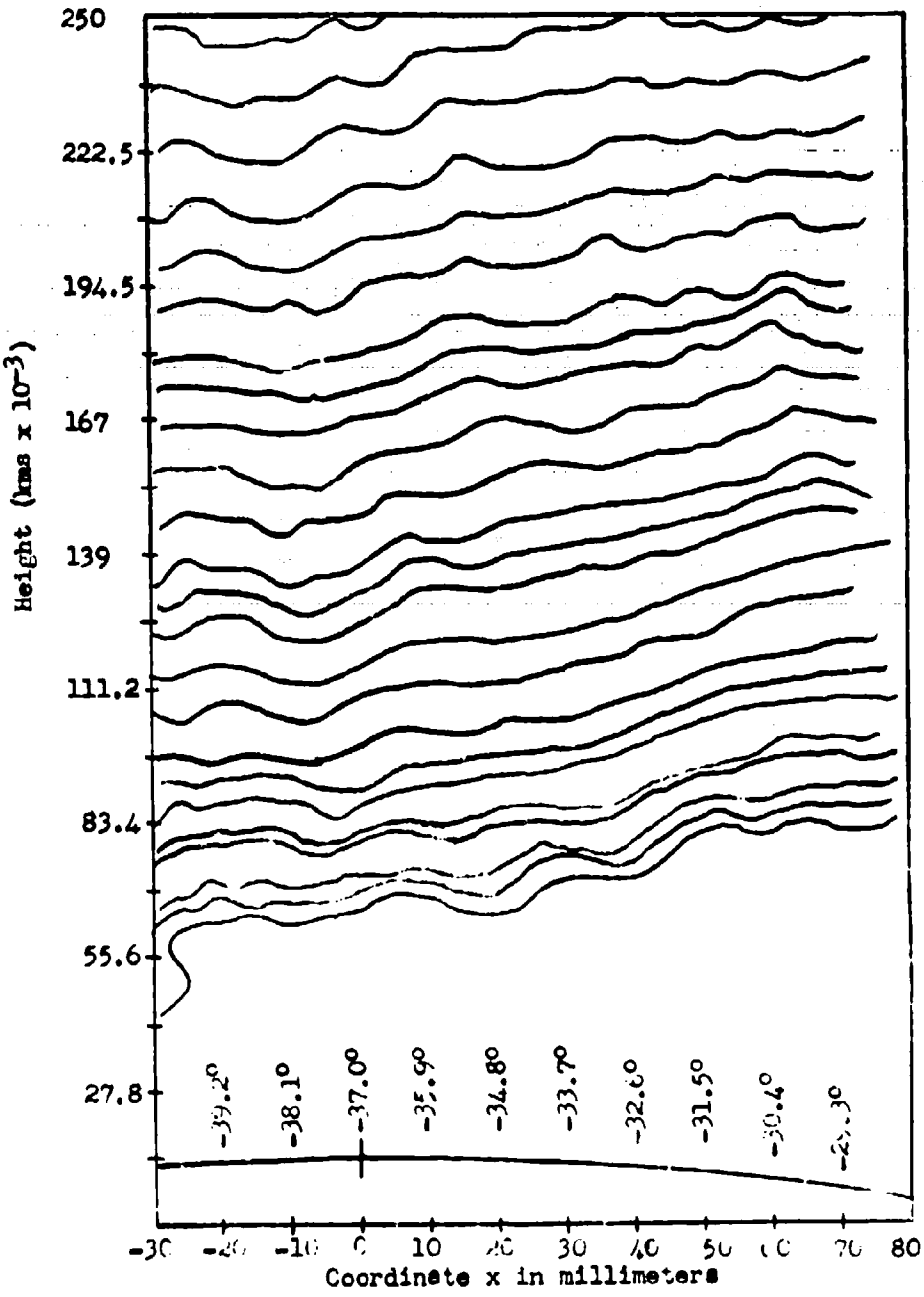

Figure 6. Showing the lower envelopes of the prominence as they were traced. The region shown is that lying between the parallel lines of figures 3 and 4. Time between any two curves is one minute.

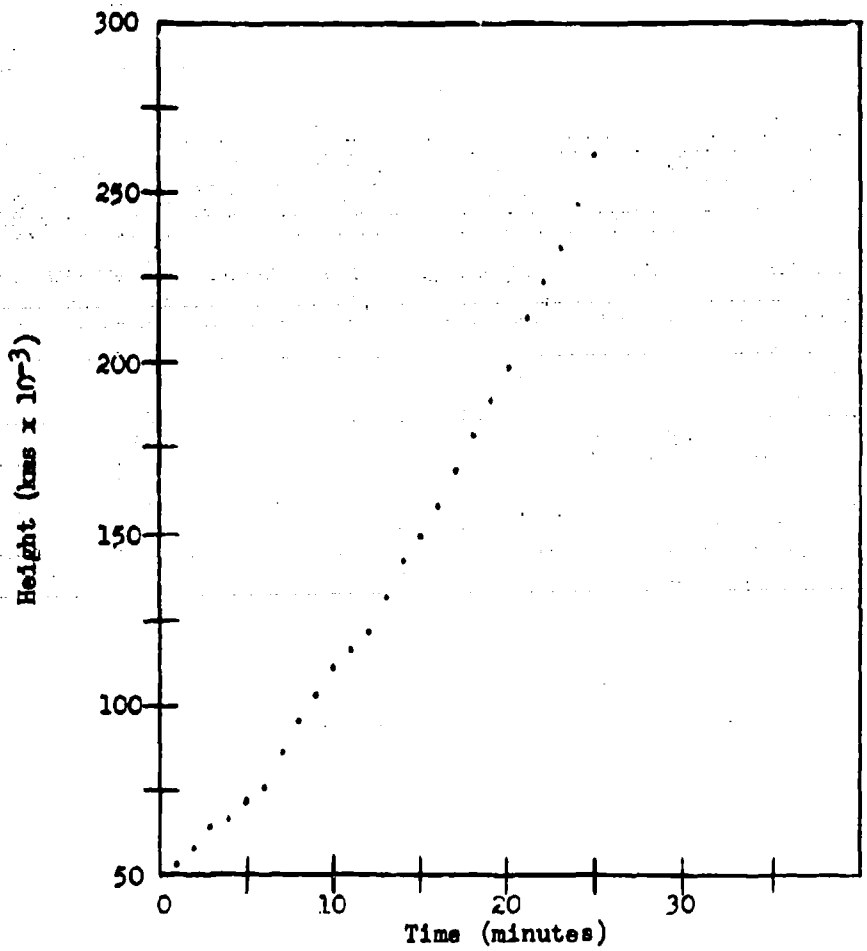

Figure 7. Plot of the vertical height (y) vs. the time along the ordinate x = 0 for the lower envelope of the prominence. Compare with figure 8.

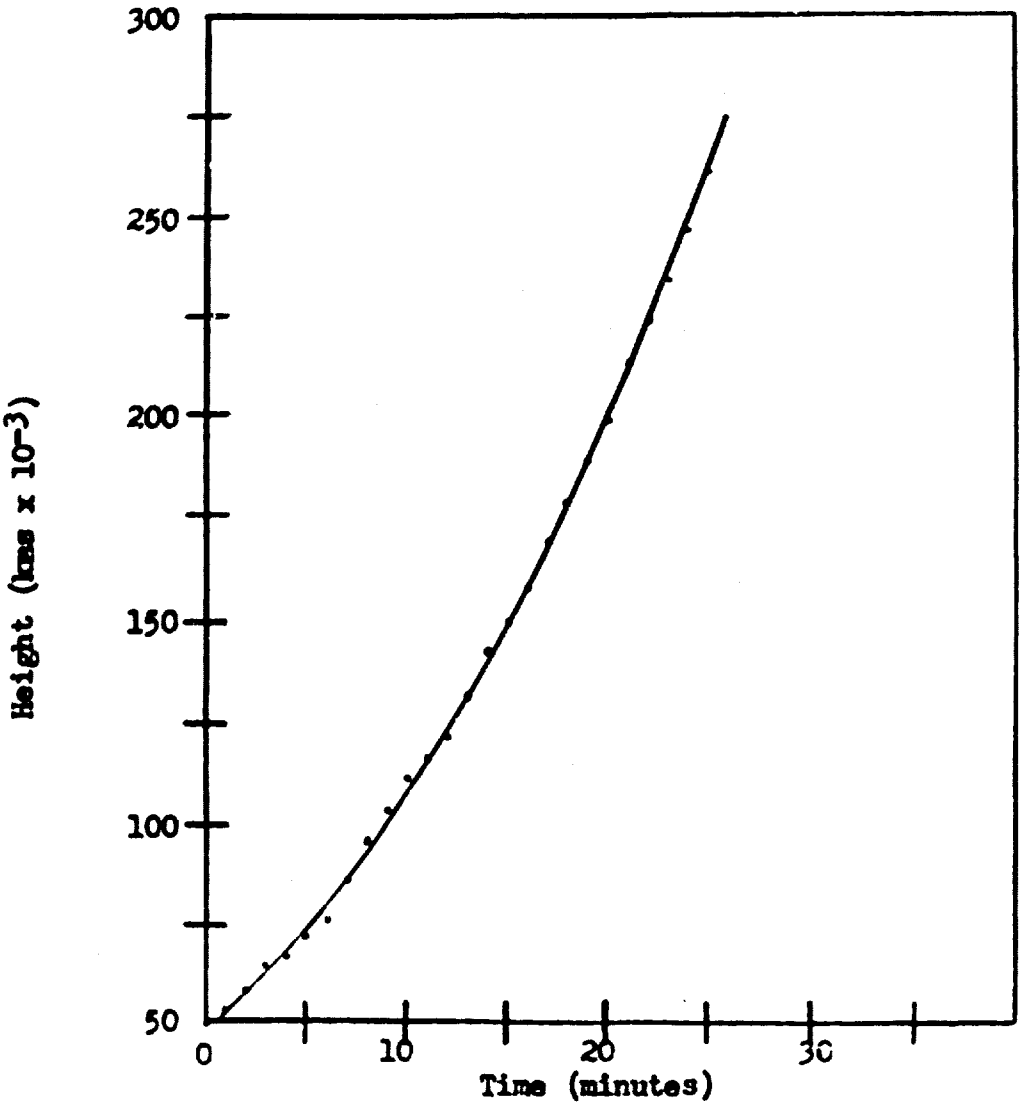

Figure 8. The smooth curve is a portion of the parabola $y = 5.00 \times 10^4 + 3.89 \times 10^3 t + 182t^2$ (kms and mins) which was obtained by applying the least squares curve fitting method of Birge. It is superimposed on the plot of the vertical height vs. the time for $x = 0$, i.e. the curve of figure 7.

paper and this error is coupled with the impossibility of reading a coordinate on the graph paper closer than approximately ± .2 mm. Thus, we see that the intrinsic uncertainty involved in determining the position of a feature in the prominence at successive intervals of time is of such magnitude as to preclude a more precise formulation of the equation of the curve.

Returning to the curves of figure 6, we note that, though the distance between them is erratic and non-uniformly increasing, they still exhibit a marked parallelism. Now, it is precisely this deviation from a uniform increase that gives rise to the humps in the curves plotted in figures 8 to 13. Concerning this situation, one might argue in the following fashion.

At any one value of x in the region, the y component of the force field might very well fluctuate in such a manner that the curve $y = y(t)$ for that value of x would be humped or in general be quite different from a parabola. Is it reasonable, then, to assume that the force field should fluctuate in precisely the same manner throughout the region of x concerned so as to produce precisely similar humps in all the $y = y(t)$ curves; that is, so that all the envelopes of the prominence in that region are markedly parallel . . . ? If so, one would be forced to admit that the force field throughout the region in question must not depend on phenomena occurring in that region; but, on the contrary, must be referred to some single source. By way of hypothetical analogy, consider the field due to a variable point charge. Were we to plot the motion of

several particles moving in this field, starting simultaneously at approximately equal distances from the particle and journeying along different radii, we would find the curves to each have the same humps and dips. Now, the hypothesis of force fields generated through the interaction of the particles of the prominence, due to their motion, that is, of force fields depending on phenomena occurring within the prominence itself, is receiving considerable attention today. In fact, some writers, notably H. Alfvén (1), have gone so far as to explain certain phases of prominence motion on this hypothesis. If, then, we must escape the conclusion that the force field has a single source, how are we to explain the parallelism displayed by the prominence envelopes? The solution becomes apparent at once when we consider the tracing process itself.

In each photograph comprising the film there is a variation in the thickness of the coronal ring appearing around the occulting disk of the coronagraph. This variation results from the positioning of the occulting disk in the photography itself. The ring is the reference point by which the previously mentioned projector is centered with respect to the coordinate axis prior to the tracing of each subsequent picture. Since the variation in the thickness of the coronal ring produces a corresponding varying brightness of the solar limb and since the limb is not clearly sharp, but somewhat diffuse, an unavoidable, undetermined error is present with each centering of the projector. We ask: is this error, coupled with the error involved in tracing the

similarly diffuse envelope of the prominence, of the same order of magnitude as the variation in the separations of the envelopes of figure 6? It is, of course, impossible to ascertain precisely the magnitude of the errors involved; but after due examination, it was decided to ascribe a value of ± 1 mm. to the uncertainty of reading a y coordinate on the graph.[6] This estimate includes the error associated with tracing and with subsequent measurement from the graph (due to the thickness of the pencil lines) and is felt to be conservative. We note carefully that this evidences only the shortcoming of the graphing procedure, and does not permit us to conclude anything about the force field. We have found, then, that from two considerations, one statistical (the Birge polynomials) and one physical (the last paragraph), that we can at best give a constant as a value for the force field by using this method.

6. 1 mm. on the graph corresponds to 1.39×10^3 kms. on the sun.

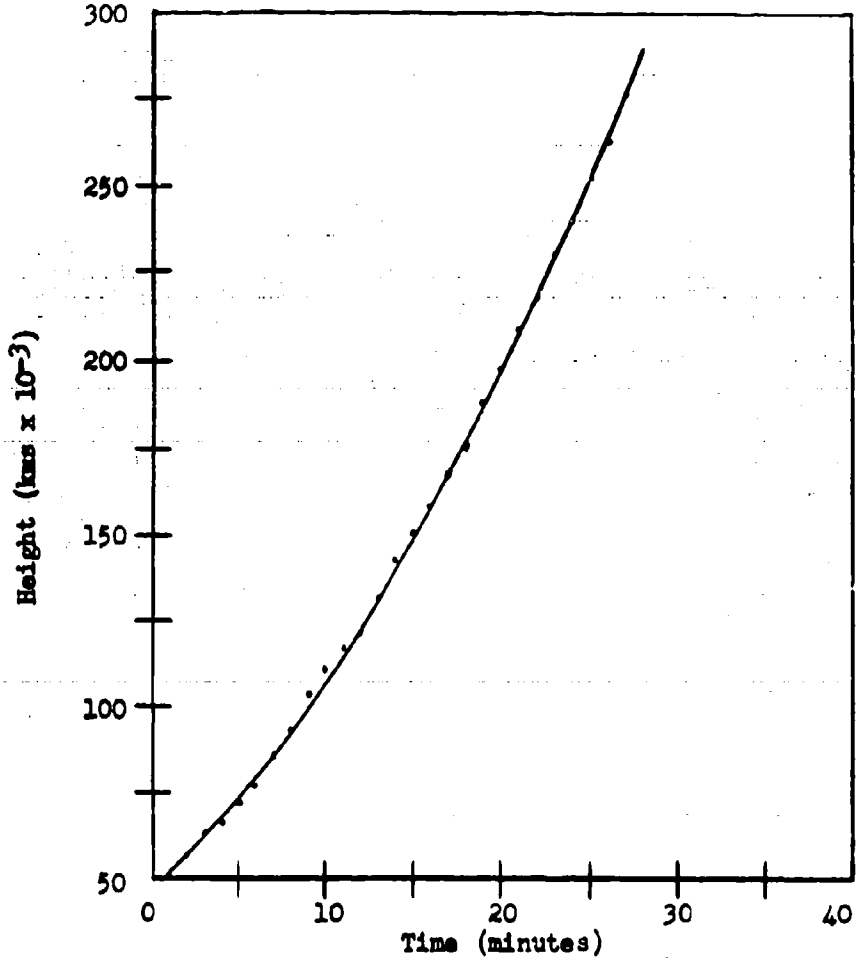

Figure 9. Illustrating the fit of the curve $y = 48 \times 10^3 + 3.62 \times 10^3 t + 129t^2$ to the observed points plotted from a measure of the height (y) vs. the time along the ordinate x = -20 for the lower envelope of the prominence.

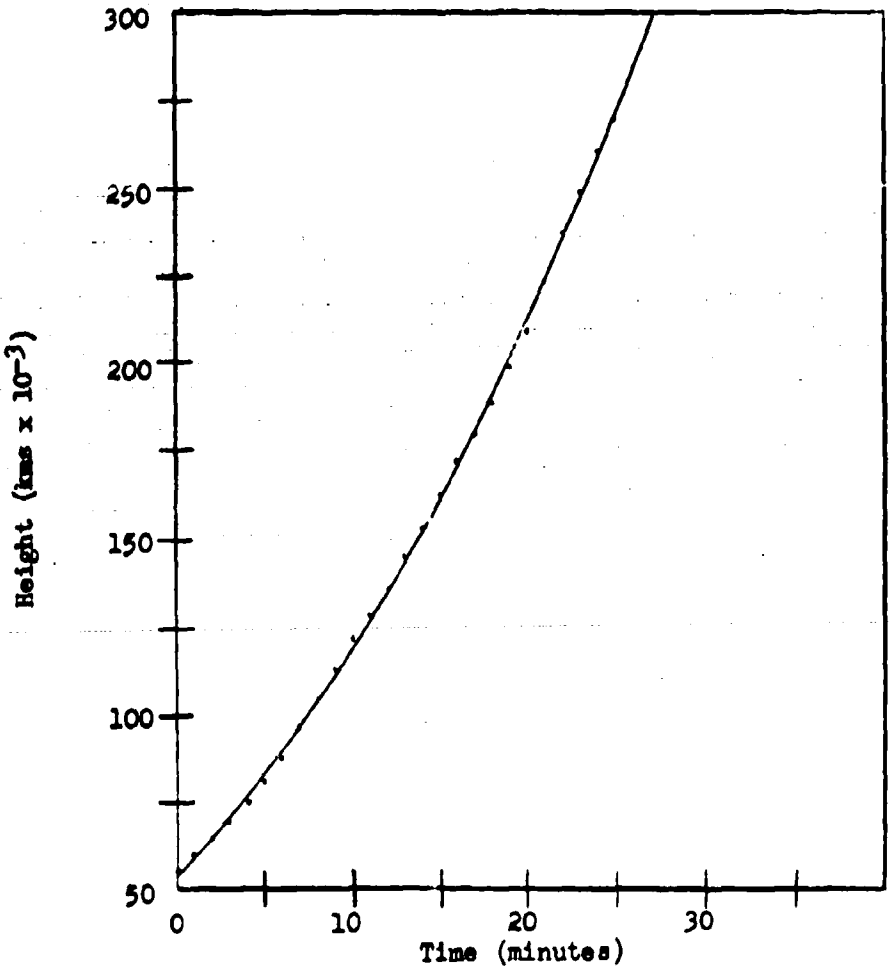

Figure 10. Illustrating the fit of the curve $y = 5.8 \times 10^4 + 3.75 \times 10^3 t + 167\ t^2$ to the observed points plotted from a measure of the height (y) vs. the time along the ordinate x = 40 for the lower envelope of the prominence.

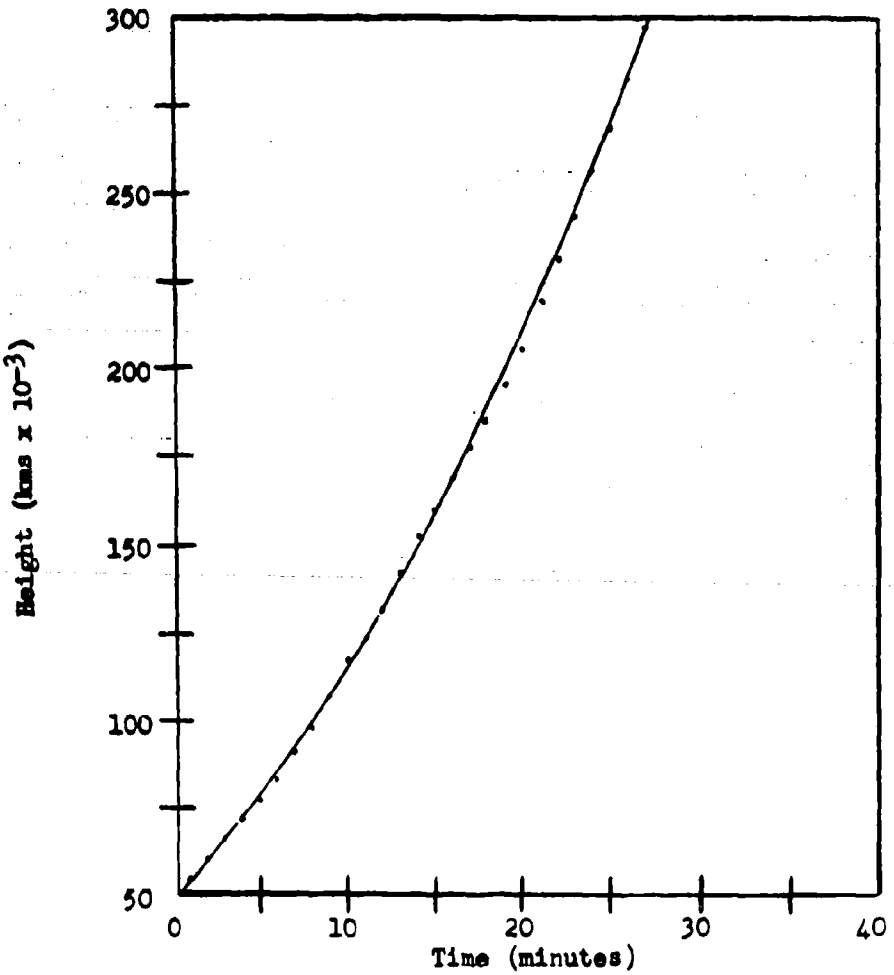

Figure 11. Illustrating the fit of the curve $y = 5.00 \times 10^4 + 4.1 \times 10^3 t + 190t^2$ to the observed points plotted from a measure of the height (y) vs. the time along the ordinate x = 20 for the lower envelope of the prominence.

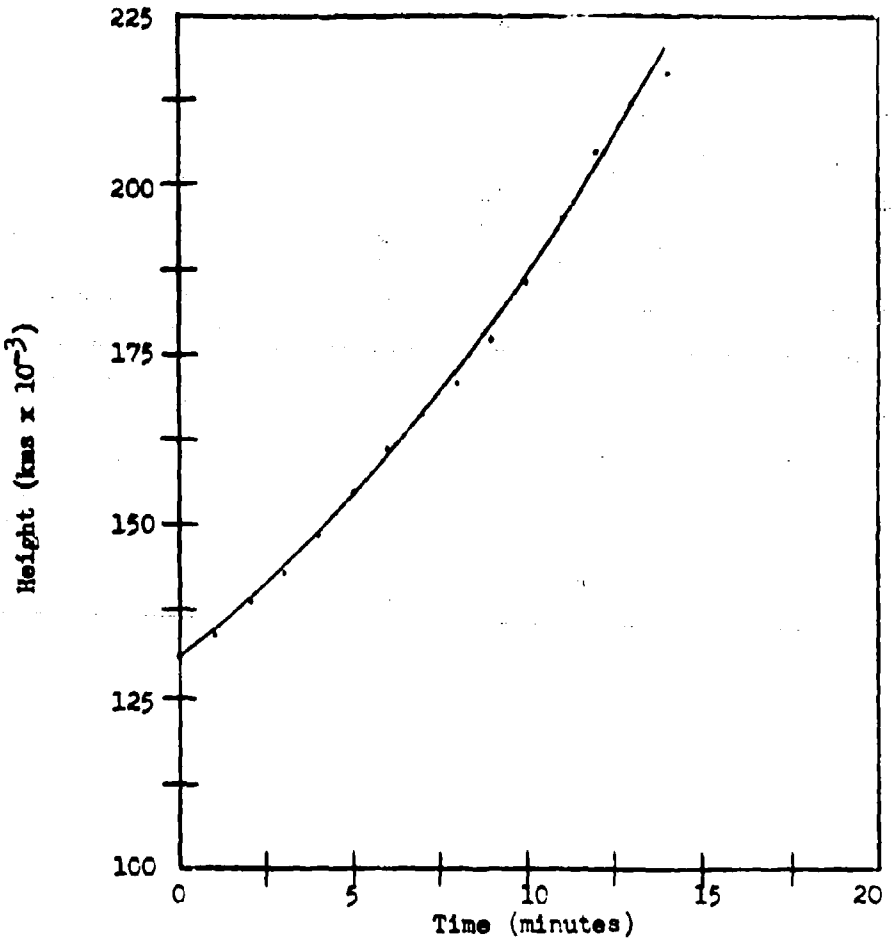

Figure 12. Illustrating the fit of the curve $y = 1.31 \times 10^5 + 3.75 \times 10^3 t + 188t^2$ to the observed points plotted from a measure of the height (y) vs. the time along the ordinate x = -20 for the upper envelope of the prominence.

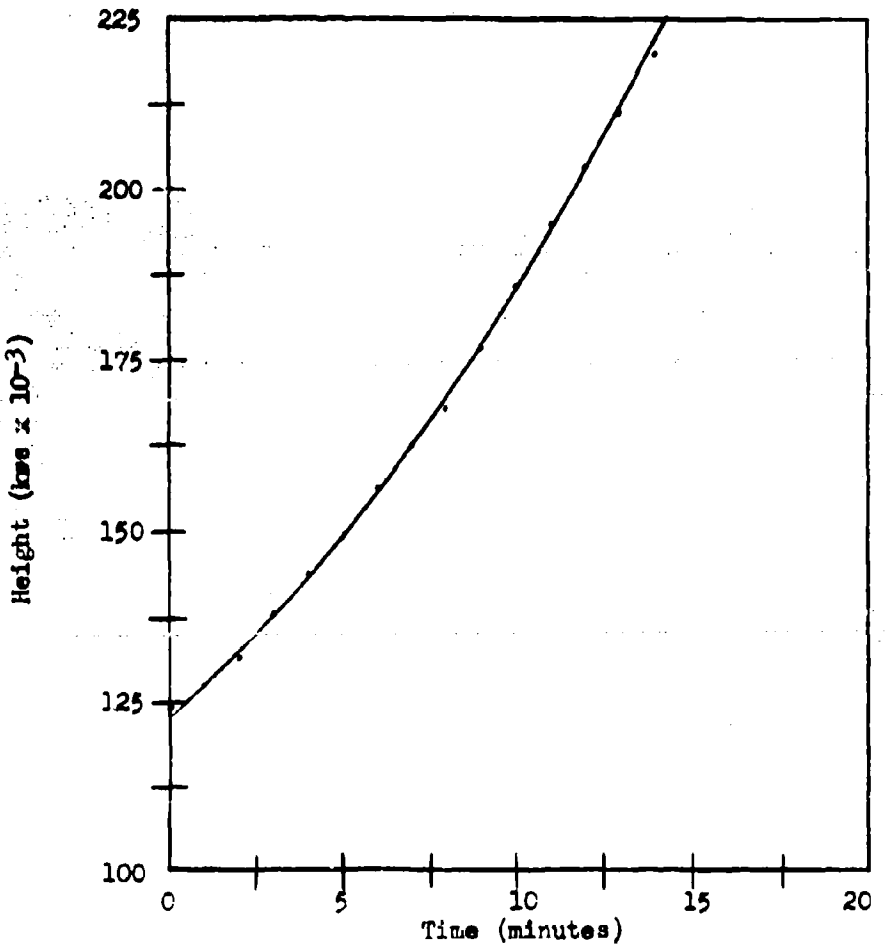

Figure 13. Illustrating the fit of the curve $y = 1.24 \times 10^5 + 4.31 \times 10^3 t + 183t^2$ to the observed points plotted from a measure of the height (y) vs. the time along the ordinate x = -30 for the upper envelope of the prominence.

Tables I through VIII contain the data measured in the region depicted in figure 6. The tolerances for the accelerations are given as calculated by the Birge method. The velocities given were measured graphically from curves such as figures 8, 9, etc.; and the tolerances listed with them are estimated values. The graphically obtained velocities are given since they describe the curve itself and may, as such, be more descriptive of the actual motion than those uniformly increasing velocities given by the Birge parabolas, which the reader can readily calculate if he so desires, using the initial position, initial velocity and the acceleration. Tables XIV through XVII list the values calculated for the upper envelopes of the prominence in the same x region as those of figure 6; and Tables IX through XIII contain the values calculated for the upper envelope describing the motion in the x direction in the region y = 40 x 10^3 to 80 x 10^3 kms, that is, the outward motion of the large southern-most column. See figures 3 and 4.

The values of x are given here as they were measured in millimeters on the graph paper, i.e., 1 mm. = 1.39 x 10^3 kms. The heliographic location for any value of x can be found from figure 6, where the solar disk is marked in degrees of latitude.

Table I. Positions, velocities and acceleration for the lower envelope of the arch as measured along the ordinate x = -20.

Time 1948 Sep. 8			$(y \pm 1.4) \times 10^3$ kms	$(V_y \pm .33) \times 10^3$ kms/min
h	m	U.T.	y	V_y
17	45.5		49.7	3.85
	47.5		57.4	4.69
	49.5		67.7	5.62
	51.5		78.4	6.36
	53.5		93.8	7.30
	55.5		113.	7.72
	57.5		123.	7.99
	59.5		144.	8.55
18	01.5		161.	9.25
	03.5		178.	9.74
	05.5		199.	10.3
	07.5		220.	10.92
	09.5		242.	11.55
	11.5		266.	13.07

Acceleration = 258 ± 110 kms/min^2
=.072 ±.030 kms/sec^2
Solar gravity = .267 kms/sec^2

Table II. Positions, velocities and acceleration for the lower envelope of the arch as measured along the ordinate x = -10.

Time 1948 Sep. 8			$(y \pm 1.4) \times 10^3$ kms	$(V_y \pm .33) \times 10^3$ kms/min
h	m	U.T.	y	V_y
17	45.5		48.7	4.01
	47.5		57.4	4.51
	49.5		67.9	5.05
	51.5		79.8	6.04
	53.5		91.7	7.16
	55.5		107.	7.72
	57.5		119.	8.28
	59.5		139.	8.76
18	01.5		157.	9.24
	03.5		174.	9.94
	05.5		193.	10.7
	07.5		220.	11.55
	09.5		243.	12.51
	11.5		263.	14.25

Acceleration = 334 ± 110 kms/min^2
= .093 ± .030 kms/sec^2

Table III. Positions, velocities and acceleration for the lower envelope of the arch as measured along the ordinate x = 0.

Time 1948 Sep. 8			$(y \pm 1.4) \times 10^3$ kms	$(V_y \pm .33) \times 10^3$ kms/min
h	m	U.T.	y	V_y
17	45.5		51.4	3.89
	47.5		58.4	4.61
	49.5		66.7	5.34
	51.5		76.5	6.06
	53.5		96.0	6.79
	55.5		110.	7.51
	57.5		122.	8.23
	59.5		143.	8.96
18	01.5		158.	9.68
	03.5		179.	11.13
	05.5		200.	11.85
	07.5		222.	12.57
	09.5		245.	13.30
	11.5		277.	14.02

Acceleration = 362 ± 117 kms/min^2
=.101 ±.033 kms/sec^2

Table IV. Positions, velocities and acceleration for the lower envelope of the arch as measured along the ordinate x = 10.

Time 1948 Sep. 8		$(y \pm 1.4) \times 10^3$ kms	$(V_y \pm .33) \times 10^3$ kms/min
h	m U.T.	y	V_y
17	45.5	54.0	3.85
	47.5	60.0	4.68
	49.5	68.0	5.62
	51.5	82.0	6.26
	53.5	99.0	6.95
	55.5	119.	7.44
	57.5	130.	7.99
	59.5	148.	8.89
18	01.5	164.	9.52
	03.5	182.	10.28
	05.5	202.	11.11
	07.5	230.	12.05
	09.5	255.	13.07
	11.5	280.	14.25

Acceleration = 380 ± 120 kms/min^2
= .105 ± .032 kms/sec^2

Table V. Positions, velocities and acceleration for the lower envelope of the arch as measured along the ordinate x = 20.

Time 1948 Sep. 8		$(y \pm 1.4) \times 10^3$ kms	$(V_y \pm .33) \times 10^3$ kms/min
h	m U.T.	y	V_y
17	45.5	50.5	4.85
	47.5	59.5	5.46
	49.5	72.0	6.04
	51.5	83.5	6.59
	53.5	98.5	7.16
	55.5	117.	7.71
	57.5	132.	8.28
	59.5	152.	9.38
18	01.5	168.	9.94
	03.5	185.	10.70
	05.5	206.	11.55
	07.5	230.	12.02
	09.5	256.	12.50
	11.5	282.	13.63

Acceleration = 380 ± 120 kms/min^2
$= .105 \pm .032$ kms/sec^2

Table VI. Positions, velocities and acceleration for the lower envelope of the arch as measured along the ordinate x = 30.

Time 1948 Sep. 8		$(y \pm 1.4) \times 10^3$ kms	$(V_y \pm .33) \times 10^3$ kms/min
h	m U.T.	y	V_y
17	45.5	58.8	3.54
	47.5	64.3	4.35
	49.5	72.8	5.24
	51.5	85.4	6.26
	53.5	102.	7.16
	55.5	121.	7.85
	57.5	135.	8.55
	59.5	152.	9.24
18	01.5	169.	9.94
	03.5	187.	10.92
	05.5	207.	12.05
	07.5	234.	12.50
	09.5	260.	13.07
	11.5	285.	13.63

Acceleration = 365 ± 117 kms/min^2
= .10: ± .031 kms/sec^2

Table VII. Positions, velocities and acceleration for the lower envelope of the arch as measured along the ordinate x = 40.

Time 1948 Sep. 8		$(y \pm 1.4) \times 10^3$ kms	$(V_y \pm .33) \times 10^3$ kms/min
h	m U.T.	y	V_y
17	45.5	57.8	4.17
	47.5	66.4	4.85
	49.5	76.3	5.62
	51.5	86.1	6.48
	53.5	94.5	7.44
	55.5	113.	8.13
	57.5	131.	8.89
	59.5	146.	9.38
18	01.5	166.	9.94
	03.5	179.	10.50
	05.5	200.	11.11
	07.5	223.	11.75
	09.5	249.	12.50
	11.5	273.	13.07

Acceleration = 334 ± 112 kms/min^2
= .093 ± .031 kms/sec^2

Table VIII. Positions, velocities and acceleration for the lower envelope of the arch as measured along the ordinate x = 50.

Time 1948 Sep. 8			$(y \pm 1.4) \times 10^3$ kms	$(V_y \pm .33) \times 10^3$ kms/min
h	m	U.T.	y	V_y
17	45.5		67.2	4.51
	47.5		74.2	5.24
	49.5		81.2	6.04
	51.5		95.2	6.59
	53.5		108.	7.16
	55.5		127.	7.58
	57.5		139.	7.99
	59.5		158.	8.40
18	01.5		173.	8.89
	03.5		191.	9.52
	05.5		211.	10.28
	07.5		234.	11.11
	09.5		259.	12.05
	11.5		283.	13.63

Acceleration = 314 ± 110 kms/min^2
= .087 ± .030 kms/sec^2

Table IX. Positions, velocities and acceleration for the upper envelope of the arch as measured along the abscissa y = 40.

Time 1948 Sep. 8		($x \pm 1.4$) x 10^3 kms	($V_x \pm .17$) x 10^3 kms/min
h	m U.T.	x	V_x
17	45.5	33.7	1.47
	47.5	36.8	1.77
	49.5	39.6	2.09
	51.5	43.1	2.22
	53.5	47.3	2.35
	55.5	52.1	2.58
	57.5	58.1	2.81
	59.5	65.3	3.02
18	01.5	74.4	3.24
	03.5	78.5	3.42
	05.5	85.5	3.58
	07.5	91.7	3.79
	09.5	98.7	4.00
	11.5	108.	4.27
	13.5	118.	4.63
	15.5	126.	4.97

Acceleration = 105 $\pm$ 32 kms/min^2
= .029 $\pm$ .009 kms/sec^2

Table X. Positions, velocities and acceleration for the upper envelope of the arch as measured along the abscissa y = 50.

Time 1948 Sep. 8			$(x \pm 1.4) \times 10^3$ kms	$(V_x \pm .17) \times 10^3$ kms/min
h	m	U.T.	x	V_x
17	45.5		29.4	1.69
	47.5		35.0	1.97
	49.5		39.2	2.26
	51.5		43.4	2.53
	53.5		49.0	2.81
	55.5		52.5	2.92
	57.5		58.8	3.02
	59.5		65.8	3.24
18	01.5		74.2	3.48
	03.5		79.8	3.65
	05.5		86.8	3.86
	07.5		92.4	4.07
	09.5		102.	4.27
	11.5		112.	4.70
	13.5		122.	5.15
	15.5		131.	5.36

Acceleration = 101 ± 29 kms/min^2
= .028 ± .008 kms/sec^2

Table XI. Positions, velocities and acceleration for the upper envelope of the arch as measured along the abscissa y = 60.

Time 1948 Sep. 8		$(x \pm 1.4) \times 10^3$ kms	$(V_x \pm .17) \times 10^3$ kms/min
h	m U.T.	x	V_x
17	45.5	18.2	2.53
	47.5	25.2	2.72
	49.5	32.2	2.92
	51.5	35.0	2.97
	53.5	42.0	3.02
	55.5	47.6	3.13
	57.5	54.6	3.24
	59.5	60.2	3.48
18	01.5	70.0	3.72
	03.5	77.0	4.00
	05.5	84.0	4.27
	07.5	91.0	4.63
	09.5	102.	4.97
	11.5	112.	5.15
	13.5	123.	5.36
	15.5	135.	5.58

Acceleration = 105 ± 26 kms/min^2
= .029 ± .007 kms/sec^2

Table XII. Positions, velocities and acceleration for the upper envelope of the arch as measured along the abscissa y = 70.

Time 1948 Sep. 8		$(x \pm 1.4) \times 10^3$ kms	$(V_x \pm .17) \times 10^3$ kms/min
h	m U.T.	x	V_x
17	45.5	09.1	2.43
	47.5	16.8	2.72
	49.5	22.4	3.02
	51.5	28.0	3.19
	53.5	36.4	3.36
	55.5	42.0	3.48
	57.5	49.0	3.58
	59.5	56.0	3.86
18	01.5	64.4	4.14
	03.5	72.8	4.38
	05.5	81.2	4.63
	07.5	87.5	4.87
	09.5	101.	5.15
	11.5	112.	5.36
	13.5	125.	5.78
	15.5	135.	6.26

Acceleration = 111 ± 29 kms/min^2
= .031 ± .008 kms/sec^2

Table XIII. Positions, velocities and acceleration for the upper envelope of the arch as measured along the abscissa y = 80.

Time 1948 Sep. 8		$(x \pm 1.4) \times 10^3$ kms	$(V_x \pm .17) \times 10^3$ kms/min
h	m U.T.	x	V_x
17	45.5	00.7	2.62
	47.5	09.8	2.81
	49.5	16.8	3.02
	51.5	21.0	3.24
	53.5	26.6	3.48
	55.5	32.2	3.58
	57.5	42.0	3.72
	59.5	47.6	4.00
18	01.5	58.8	4.27
	03.5	65.8	4.63
	05.5	77.0	4.97
	07.5	84.	5.36
	09.5	98.	5.78
	11.5	109.	6.02
	13.5	122.	6.26
	15.5	133.	6.54

Acceleration = 123 ± 35 kms/min^2
= $.034 \pm .009$ kms/sec^2

Table XIV. Positions, velocities and acceleration for the upper envelope of the arch as measured along the ordinate x = 0.

Time: Sep 8 1948 h	m U.T.	$(y \pm 1.4) \times 10^3$ kms y	$(V_y \pm .33) \times 10^3$ kms/min V_y
17	45.5	119	3.86
	47.5	128	4.52
	49.5	139	5.36
	51.5	155	6.02
	53.5	164	6.82
	55.5	182	7.82
	57.5	203	9.05
	59.5	217	10.71

Acceleration = 397 ± 61 kms/min^2 = .110 ± .017 kms/sec^2

Table XV. Positions, velocities and acceleration for the upper envelope of the arch as measured along the ordinate x = -10.

Time: Sep 8 1948 h	m U.T.	$(y \pm 1.4) \times 10^3$ kms y	$(V_y \pm .33) \times 10^3$ kms/min V_y
17	45.5	117	3.36
	47.5	130	4.00
	49.5	148	4.77
	51.5	160	5.36
	53.5	168	6.02
	55.5	183	6.82
	57.5	202	7.82
	59.5	217	8.60

Acceleration = 357 ± 54 kms/min^2 = 099 ± .015 kms/sec^2

Table XVI. Positions, velocities and acceleration for the upper envelope of the arch as measured along the ordinate x = -20.

Time: Sep. 8 1948 h	m U.T.	$(y \pm 1.4) \times 10^3$ kms y	$(V_y \pm .33) \times 10^3$ kms/min V_y
17	45.5	133	3.72
	47.5	140	4.28
	49.5	149	4.98
	51.5	163	5.67
	53.5	172	6.54
	55.5	188	7.20
	57.5	206	8.18
	59.5	220	9.54

Acceleration = 377 ± 64 kms/min^2 = .104 ± .017 kms/sec^2

Table XVII. Positions, velocities and acceleration for the upper envelope of the arch as measured along the ordinate x = -30.

Time: Sep 8 1948 h	m U.T.	$(y \pm 1.4) \times 10^3$ kms y	$(V_y \pm .33) \times 10^3$ kms/min V_y
17	45.5	126	4.31
	47.5	134	5.04
	49.5	144	5.79
	51.5	158	6.50
	53.5	169	7.23
	55.5	188	7.97
	57.5	206	8.70
	59.5	223	9.43

Acceleration = 366 ± 70 kms/min^2 = .105 ± .020 kms/sec^2

CONCLUSION

We have seen that the measurements obtained by plotting the motion of the prominence envelopes and analyzing these by means of a least squares method of curve fitting has predicted that the force field under which the prominence was expanding was a constant one, at least in so far as the material is moving upward with a constant vertical component of acceleration. Obviously, the acceleration can not be constant; for, if it were, the material of the prominence would continue to rise and recede to infinity. Remembering the relatively short time interval during which measurements were made, it seems natural to conclude that the acceleration was actually changing slowly, but that the total change which had occurred during the period of measurement was too small to be detected by our method with its relatively large experimental error. Furthermore, the acceleration measured in the central region of the prominence, i.e., that between the parallel lines of figures 2 and 3 is only the vertical component; while study of the motion picture film suggests strongly that material is actually streaming downward along the arches, and it seems largely for this reason that the arch has been so greatly dispersed by 18^h15^m (figure 4).

The critical velocity of escape of a body leaving the surface of the sun, and thereafter being subject only to gravitation, is 615 kms/sec. This value, however, applies only when the body is not influenced by any forces other than gravity, following its instant of departure. For bodies which have been supported far above the chromosphere, by some means,

the value of the critical escape velocity, of course, falls off inversely as the square root of the distance from the center of the sun. However, a simple calculation readily indicates that the body must be several hundred thousand kilometers above the chromosphere before there is an appreciable change in the value of the critical velocity of escape. We have seen that the solar prominence of September 8, 1948 had attained a vertical velocity of 250 kms/sec by 18^h15^m. Thus it would seem that the likelihood that any portion of it completely escaped solar gravity and receded into space is a slight one, at least in so far as visible material is concerned. It is generally felt that, although eruptive prominences go far out into coronal space, they disintegrate there and their atoms eventually return to the sun.

It is noteworthy that the results of our measurements apparently give no evidence in support of the laws of prominence motion.[7] This is particularly noticeable in the case of the second law; and it was, to a large extent, for the purpose of testing this law that the velocities were measured graphically, in order that they conform as nearly as possible to the observed motion.

At this writing, there are under construction new coronagraphs to be used at the High Altitude Observatory, Climax, Colorado and the Upper Air Research Observatory of USAF at Sacramento Peak, New Mexico (soon to

---

7. Originally formulated by Edison Pettit, the laws are as follows:
1st law: Prominence motion is uniform, increasing suddenly at intervals.
2nd law: Successive velocities are small whole number multiples of the preceding (or second preceding). See literature consulted (20), (21), (22).

be put into operation). The difficulty involved in the centering of the occulting disk has been eliminated in these new instruments and they will undoubtedly supply us with some very accurate measurements. The method of envelope tracing should yield some interesting results in the not too distant future.

LITERATURE CONSULTED

1. Alfvén, Hannes, "Cosmical Electrodynamics" Oxford, Clarendon Press, (1950).

2. The American Ephemeris and Nautical Almanac, 399, 629 (1948).

3. Birge, Raymond T., "The Propogation of Errors", Am. Phys. Teacher, 7, 351 (1929).

4. Birge, Raymond T., "Least Squares Fitting of Data by Means of Polynomials", Rev. Mod. Phys., 19, 298-360 (1947). Appendix by J. W. Weinberg.

5. Birge, Raymond T., and Shea, J. D., "Least Squares Fitting of a Polynomial of any Degree", Phys. Rev., 24, 206A (1924).

6. Chapman, Sydney, and Bartels, Julius, "Geomagnetism", Oxford Press, Vol. I, 160-170 (1940).

7. Deming, W. Edwards, "Some Notes on Least Squares", Graduate School of the Dept. of Agriculture, 27-28.

8. Deming, W. Edwards, and Birge, Raymond T., "On the Statistical Theory of Errors", Rev. Mod. Phys., 6, 147-149 (1934).

9. Dodson, Helen W., "A General Study of a Prominence Field", M. N. 108, 384-398 (1948).

10. Dodson, Helen W., and Donselman, Robert W., "The Eruptive Prominence of August 7, 1950", Ap. J., 113, 519 (1951).

11. Dodson, Helen W., and McMath, Robert J., "Solar Filament of December 7, 1948", PASP, 60, 366 (1948).

12. Dodson, Helen W., and Weston, Edwin B., "A Study of the Eruptive Prominence of 1948 September 27", M. N., 110, 199-206 (1950).

13. Leland, Ora Miner, "Practical Least Squares", McGraw-Hill, 178-180, (1921).

14. Lyot, Bernard, "Photographie de la Couronne Solaire en Dehors des Eclipses", Comptes Rendus, 193, 1169 (1931).

15. McMath, Robert R., "The Surface of the Nearest Star", Sci. Mo., 47, 418 (1938).

16. Mansel, Donald H., "Our Sun", Blakiston's Sons and Co., Philadelphia (1949).

17. Mansel, Donald H., "Origin of Sunspots", Nature, 166, 31 (1951).

18. Merriman, Mansfield, "Method of Least Squares", John Wiley and Sons Inc., New York, 66-80 (1915).

19. Pettit, Edison, "The Highest Eruptive Prominence", Sci. Mo., 47, 421-428 (1938).

20. Pettit, Edison, "The Possible Escape of Prominences from the Sun", PASP, 52, 172 (1940).

21. Pettit, Edison, "The Motions of Prominences of the Eruptive and Sunspot Type", Ap. J., 84, 319, 336, 339, 343 (1936).

22. Pettit, Edison, and McMath, Robert R., "Prominences of the Active and Sunspot Type Compared", Ap. J., 85, 296 (1937).

APPENDIX A

THE HELIOGRAPHIC COORDINATE SYSTEM AND THE LOCATION OF THE SUNSPOTS AND SOLAR PROMINENCE OF SEPTEMBER 8, 1948

The heliographic coordinate system, devised by Carrington[8] in 1863 describes the sun's position at any date by means of three coordinates which are defined as follows:

P = the position angle of the axis of rotation measured positively eastward from the north point of the disk.

B_o = the heliographic latitude of the center of the disk.

L_o = the heliographic longitude of the center of the disk reckoned from the solar meridian positively to the west.

Solar meridian = that longitudinal line which passed through the ascending node of the sun's equator on the ecliptic, January 1, 1854.

From the U. S. Naval Observatory Circular 6, December 19, 1949, page 8, we obtain the following tabular data:

Mount Wilson No.	Date	Lat.	Difference in Long.[9]	Distance from Center	Area	Spot Count
N-O-F 9395	Sept 9.633	-24	-65			1
N-O-F 9400 (a)	Sept 15.640	- 2	-27		388	2
9400 (b)	Sept 15.640	-6	-27	-34	97	

8. Richard Christopher Carrington (1826-1875), English astronomer, see American Ephemeris and Nautical Almanac (2) and the Encyclopedia Britannica, Volume IV, 1952.
9. Measured from the central meridian.

And from the Publications of the Astronomical Society of the Pacific, December 1948, Vol. 60, No. 357, p. 389:

Sept. 14.4

No. 9395 lat. -23 first seen Sept. 8 1βd

Sept. 15.9

No. 9400 lat. -26 first seen Sept. 10 1βp1

Furthermore, we know that the "position angle" of the prominence origin, which is defined as the angle subtended by a vertical line and a line through the prominence, intersecting the vertical in the center of the disk and measured positively in a counter clockwise direction, is 150°. From the American Ephemeris and Nautical Almanac (2), we find for Sept. 8, 1948:

$$L_0 = 58.29^\circ$$

$$B_0 = 7.25^\circ$$

$$P = 22.78^\circ$$

From figure 14, which depicts graphically the position of the sun on Sept. 8, 1948, and using the above values of the coordinates, we see that solution of the spherical triangle ABC for side x will enable us to find the heliographic latitude of the prominence. By the law of cosines, we have:

$$\cos x = \cos(82.75)\cos(90) + \sin(90)\sin(82.75)\cos(127.22) = -.602$$

$$x = \cos^{-1}(-.602) = -127^\circ$$

Hence, the heliographic latitude of our origin is -37°. Solar longitude is measured positively to the west and hence the heliographic longitude of the limb and thus of the prominence is $270^\circ + L_0 = 270^\circ + 58.29^\circ = 328.29^\circ$ or about 328° for Sept. 8, 1948.

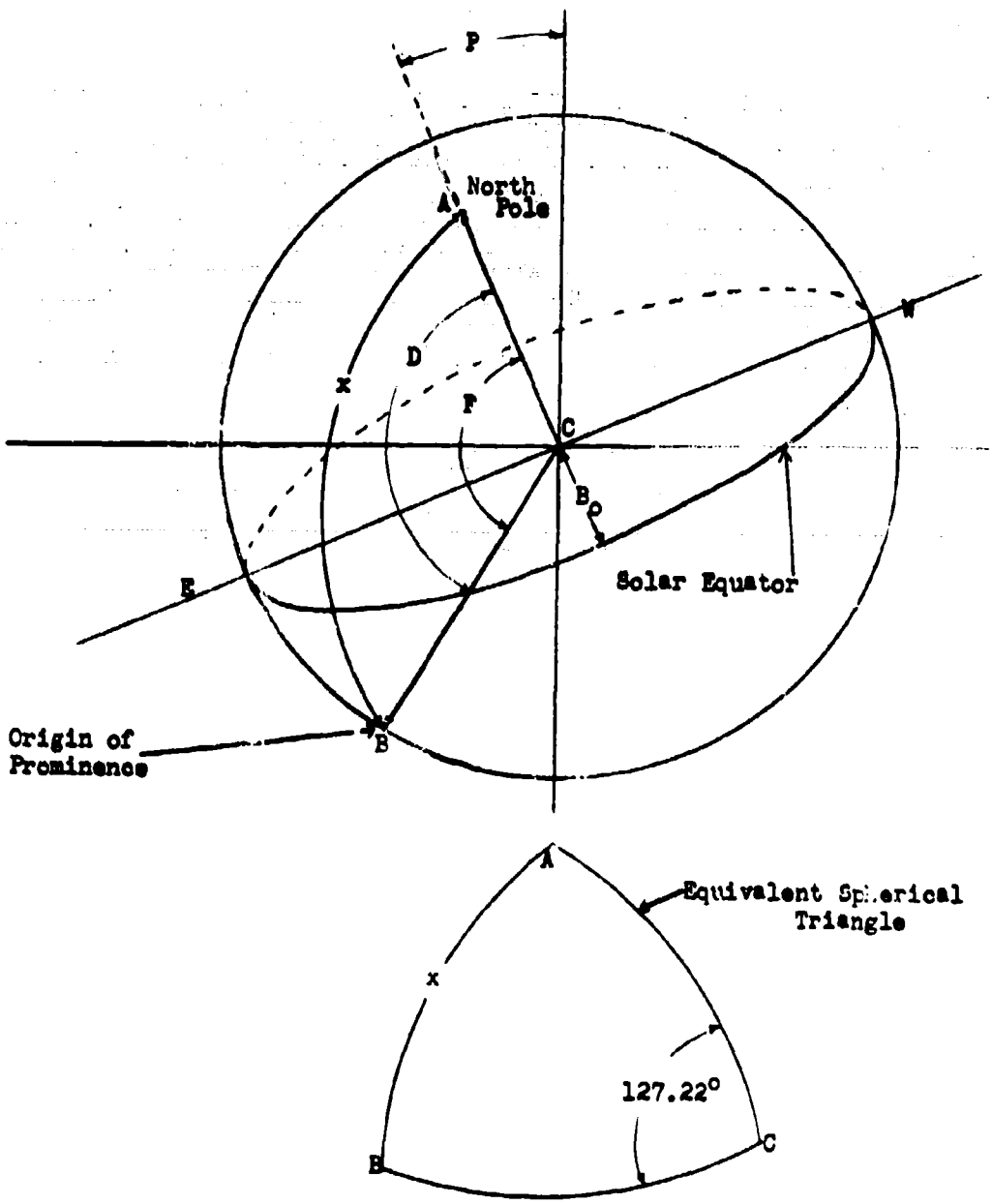

Figure 14. Illustrating Carrington's coordinates and the spherical triangle procedure used in finding the latitude of the solar prominence. D = 150°; F = 150°-P; P = 22.78°; B_o = 7.25°; arc AC = 90° - B_o; arc BC = 90°.

On Sept. 15.640, we find Mount Wilson No. 9400a was 6° east of the central meridian with a latitude of -27°, but the time of measurement was about Sept. 8.83. The sun rotates on its axis at a rate of approximately one revolution in 25.36 days or about 14.197° per day. However, due to the well known "equatorial acceleration" of solar rotation, sunspots near the 35th parallel have a diurnal rotation of approximately 13.51°. Calculating from this, we find on Sept. 8.83, No. 9400a was at -2° - 88° or at -90° (on the eastern limb)[10]. No. 9400b was at -6° -88° or at -94° (behind the limb), and No. 9395 was at -65° -13° = 78° (or on the disk 12° from the limb).

From the graph, we find the southern-most extremity of the arch at -65 mm. from the origin or at -91.0×10^3 kms. solar distance, which corresponds to approximately 7.5° of arc to the south of the origin. This would place the southern arch at about -44.5° heliographic latitude. The northern-most branch of the arch meets the chromosphere at about 120 mm. or 167.3×10^3 kms. solar distance, which corresponds to 14° of arc on the limb and places the northern extremity at approximately -23° heliographic latitude.

---

10. Compare with footnote 9; i.e., these angles are not heliographic longitude, but are measured from the central meridian.

APPENDIX B

CALCULATION OF THE ANALYTICAL EQUATION OF THE BEST FIT CURVE FOR THE OBSERVED POINTS OF FIGURE 7

The Least Squares Orthogonal Polynomial method of curve fitting as adapted by Raymond T. Birge and J. W. Weinberg is, for the purpose of illustration, applied here to the points representing the measurements of the height (y coordinate) at equally spaced intervals of time along the ordinate x = 0. The following table presents the measured y coordinates, reading successively downward in the Y_{-q} column and upward in the Y_q column in that order. The columns headed $Y_q - Y_{-q}$ and $Y_q + Y_{-q}$ contain the differences and sums of the numbers appearing in the Y_q and Y_{-q} columns. The V's are "pair factors" of a system of orthogonal polynomials and are given in the Birge tables for any number of observations up to 29. The row labeled N_t contains the statistical weights of the coefficients b_t and is also given in the Birge tables. The following four rows are calculated as indicated by the formulas. The row labeled ΣYV_t contains the sums of the products of the V's and the columns $Y_q - Y_{-q}$ and $Y_q + Y_{-q}$ to the left and right respectively. In the case of the column headed t = 0, the value of K_t is simply the sum of the numbers in that column.

TABLE XVIII

TABLE OF VALUES TO BE USED IN THE CALCULATION OF THE EQUATION OF THE BEST FIT CURVE FOR THE OBSERVED POINTS OF FIGURE 7

$y = f(t)$ $x = 0$ $n = N_o = 29$ $h = 60$ $m = 14 \times 60$

t = 5	3	1				0	2	4
V_5	V_3	V_1	$Y_4 - Y_4$	Y_4	Y_4	$Y_4 + Y_4$	V_2	V_4
8190	819	14	182	37	219	256	126	4095
-585	468	13	168	39	207	247	99	1170
-4810	182	12	156	42	198	240	74	-780
-5885	-44	11	140	47	188	235	51	-1930
-4958	-215	10	130	48	178	226	30	-2441
-2946	-336	9	115	53	167	222	11	-2460
-556	-412	8	105	55	160	215	-6	-2120
1694	-448	7	92	62	154	215	-21	-1540
3454	-449	6	75	69	144	213	-34	-825
4521	-420	5	63	73	135	209	-45	-66
4818	-366	4	50	79	129	208	-54	660
4373	-292	3	36	84	120	204	-61	1290
3298	-203	2	27	88	115	203	-66	1775
1768	-104	1	16	95	111	206	-69	2080
000	000	0	—	—	103	103	-70	2184
500,671,080	4,207,320	2,030	—	N	—	29	113,274	107,987,880
-15,800	3,770	13,100	—	$\Sigma Y V_t = K_t$	—	3,200	14,700	39,100
-3.16×10^{-5}	8.95×10^{4}	6.45	—	$b_t = \frac{K_t}{N_t}$	—	1.10×10^{2}	1.30×10^{-1}	3.62×10^{-4}
9.98×10^{-10}	80.1×10^{8}	41.6	—	b_t^2	—	1.21×10^{4}	1.69×10^{-2}	13.1×10^{-3}
.50	3.37	8.4448×10^{4}	—	$N_t \cdot b_t^2$	—	3.509×10^{5}	1.914×10^{3}	14.14

The following calculations give the successive values of $\sum v_j^2$ and represents the determination of the degree of the equation to be used. Note that there is no appreciable change in the value of $\sum v_j^2$ after the third subtraction, indicating that a second degree equation should fit the observed points very nearly as well as a third, fourth, or fifth degree equation. The value of $(\sum v_i^2)^{\frac{1}{2}}$ is used later in the calculation of the probable error.

$$\sum y^2 = 440,376.27$$
$$-N_0 b_0^2 = \underline{350,900.00}$$
$$\sum v_0^2 = 89,476.27$$
$$-N_1 b_1^2 = \underline{84,448.00}$$
$$\sum v_1^2 = 5,028.27$$
$$-N_2 b_2^2 = \underline{1,914.33}$$
$$\sum v_2^2 = 3,113.94$$
$$-N_3 b_3^2 = \underline{\quad 3.37}$$
$$\sum v_3^2 = 3,110.57$$
$$-N_4 b_4^2 = \underline{\quad 14.14}$$
$$\sum v_4^2 = 3,096.43$$
$$-N_5 b_5^2 = \underline{\quad .50}$$
$$\sum v_5^2 = 3,095.93$$

For a polynomial $y_j(t) = \sum_{k=0}^{j} a_{kj} t^k$, the coefficients a_{kj} as calculated by the least squares method of Birge and Weinberg are given by $a_{kj} = \sum_{t=k}^{n} H_{kt} b_t$.

Here the numbers b_t are simply those calculated in Table X. The coefficients H_{kt} are calculated as follows: (The values of S_{ij}, as given for n = 29, are supplied by the Birge tables.)

$$H_{oo} = S_{oo} = 1$$

$$H_{o1} = -S_{11}(m/h)^2 = -14$$

$$H_{o2} = S_{o2} + S_{22}(m/h)^2 = 126$$

$$H_{11} = S_{11}/h = 1/60$$

$$H_{12} = -S_{22}(2m/h^2) = -8/60$$

$$H_{22} = S_{22}/h^2 = 1/60^2$$

Hence, corrected to graphical scale, the coefficients are:

$$a_{o2} = 36.0 \times 1.39 \times 10^3 = 5.00 \times 10^3 \text{kms.}$$

$$a_{12} = \frac{2.80}{60} \times 1.39 \times 10^3 \times 60 = 3.89 \times 10^3$$

$$a_{22} = \frac{.130}{60^2} \times 1.39 \times 10^3 \times 60^2 = 181$$

Thus the equation of the best fit curve through the points of figure 7 is: $y = 5.00 \times 10^3 + 3.89 \times 10^3 t + 181t^2$ (kms. and mins.)

The probable error of the coefficients is given by:

$$r_{kj} = r_j' (1/p_{kj})^{\frac{1}{2}}$$

where: $1/p_{kj} = \sum_{t=k}^{n} (H_{kt}^2 / N_t)$ and: $r_j' = .6745 \left[\frac{\sum v_j^2}{n-(j+1)} \right]^{\frac{1}{2}}$

The values of H_{kt}, N_t, and $\sum v_j^2$ are given above. Substituting and

carrying out the calculations, we find:

$$r_{aa} = 38.5$$

r_{aA} and r_{AA} are not calculated since the positions and velocities as presented in the tables were both measured directly from the graphs and their probable errors were calculated in a corresponding manner.